

22. ^{40}Ar - ^{39}Ar INVESTIGATION OF VOLCANIC CLASTS IN GLACIOGENIC SEDIMENTS AT SITES 1097 AND 1103 (ODP LEG 178, ANTARCTIC PENINSULA)¹

G. Di Vincenzo,² A. Caburlotto,³ and A. Camerlenghi³

ABSTRACT

Three selected diamictite samples recovered within sequence group S3 at Sites 1097 (Sample 178-1097A-27R-1, 35–58 cm) and 1103 (Samples 178-1103A-31R-2, 0–4 cm, and 36R-3, 4–8 cm) of Ocean Drilling Program Leg 178 have been investigated by scanning electron microscope, electron microprobe, and ^{40}Ar - ^{39}Ar laser-heating techniques. They contain variable proportions of fragments of volcanic rock groundmass (mostly in the range of 100–150 μm) with textures ranging from microcrystalline to ipocrystalline. Their rounded shapes indicate mechanical reworking. Fresh groundmass glasses, recognized only in grains from samples of Site 1103, show mainly a subalkaline affinity on the basis of total alkali-silica variations. However, they are characterized by relatively high TiO_2 and P_2O_5 contents (1.4–2.8 and 0.1–0.9 wt%, respectively). Because of the small size of homogeneous grains (100–150 μm), they were not suitable for single-grain total fusion ^{40}Ar - ^{39}Ar analyses. The incremental laser-heating technique was applied to milligram-sized samples (only for Samples 178-1097A-27R-1, 35–58 cm, and 178-1103A-36R-3, 4–8 cm) and to various small fractions (each consisting of 10 grains for the sample from Site 1097 and 30 grains for samples from Site 1103). The latter approach resulted in more effective resolution of sample heterogeneity. Argon ages from the small fractions show significantly different ranges in the three samples: 75–173 Ma for Sample 178-1097A-27R-1, 35–58 cm, 18–57 Ma for Sample 178-1103A-31R-2, 0–4 cm, and 7.6–50 Ma for Sample 178-1103A-36R-3, 4–8 cm. Ca/K ratios

¹Di Vincenzo, G., Caburlotto, A., and Camerlenghi, A., 2001. ^{40}Ar - ^{39}Ar investigation of volcanic clasts in glaciogenic sediments at Sites 1097 and 1103 (ODP Leg 178, Antarctic Peninsula). In Barker, P.F., Camerlenghi, A., Acton, G.D., and Ramsay, A.T.S. (Eds.), *Proc. ODP, Sci. Results*, 178, 1–26 [Online]. Available from World Wide Web: <http://www-odp.tamu.edu/publications/178_SR/VOLUME/CHAPTERS/SR178_22.PDF>. [Cited YYYY-MM-DD]

²Istituto di Geocronologia e Geochimica Isotopica-CNR, via Moruzzi, 1, I-56124 Pisa, Italy.
G.DiVincenzo@iggpi.cnr.it

³Istituto Nazionale di Oceanografia e di Geofisica Sperimentale-OGS, Borgo Grotta Gigante 42/c, Sgonico I-34010 Trieste, Italy.

Initial receipt: 26 January 2001

Acceptance: 20 July 2001

Web publication: 1 November 2001
Ms 178SR-232

derived from argon isotopes at Site 1103 suggest that the data mainly refer to outgassing of groundmass glass. At Site 1103, we observe an overall apparent age increase with decreasing sample depth. This is compatible with glacial erosion that affected with time deeper levels of a volcanic sequence previously deposited on the continent. The youngest apparent age of 7.6 ± 0.7 Ma detected close to the bottom of Hole 1103A (340 meters below seafloor [mbsf]) is compatible with the age range of the diatom *Actinocyclus ingens v. ovalis* Zone (6.3–8.0 Ma) determined for the interval 320–355 mbsf and with the maximum ages derived from strontium isotope composition of barnacle fragments obtained at 262–263 mbsf at the same site. Nevertheless, this age cannot be taken as the maximum youngest age of the volcanic sequence sampled by glacial erosion or as the maximum age for the deposition of the Sequence S3 at 340 mbsf unless validated by further research.

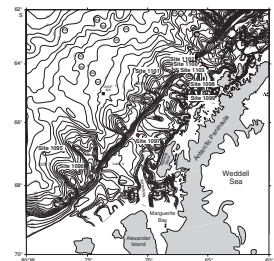
INTRODUCTION

The Antarctic Peninsula has been a major active margin for at least 200 m.y., with subduction of Pacific oceanic lithosphere beneath continental lithosphere along the west coast of the peninsula. As a consequence of a series of spreading center–trench collisions, subduction ceased during the Cenozoic progressively northward, from ~50 Ma in the southern sector of the margin to ~4 Ma in the northern part (Barker, 1982). After cessation of subduction, magmatism continued with intraplate basaltic rocks erupted from centers scattered along the whole Antarctic Peninsula (e.g., Hole, 1990; Smellie, 1999). This long-lived igneous activity makes the Antarctic Peninsula a region where the magmatic record may be used to place timing constraints on paleoenvironmental evolution during the Cenozoic.

Analogous to other continental margins of the world, the Antarctic margin records a long-term history of Cenozoic oceanographic changes and sedimentary processes. Ocean Drilling Project (ODP) Leg 178 was the first drilling campaign of the *JOIDES Resolution* aimed at the reconstruction of the history of the Antarctic ice sheet, as proposed by ANTOSTRAT (Antarctic Offshore Acoustic Stratigraphy) initiative (Barker and Camerlenghi, 1999) (Fig. F1). However, the presence of a polar ice sheet as the main agent of sediment erosion, transport, and deposition introduces elements of uncertainty into the interpretation of the drilling record. The distribution of sedimentary bodies on the continental shelf is not primarily controlled by sea level, because the waxing and waning of the ice sheet has overdeepened the seafloor surrounding the continent to depths in general greater than 500 m, well outside the range of Cenozoic eustatic changes. The sediments do not generally contain a continuous record of microfossils. Periodic advances of grounded ice sheets alternate erosion to deposition and the sediments deposited are mostly unsorted terrigenous sediments (diamicts).

During ODP Leg 178, we drilled the Pacific margin of the Antarctic Peninsula based on seismic stratigraphic information collected over the years. It was recognized, as it turned out, that (1) large sediment drifts on the proximal continental rise contain a continuous and expanded sedimentary record sensitive, indirectly, to ice sheet fluctuations on the continental shelf; (2) the continental shelf contains a discontinuous sedimentary record as direct evidence of past ice sheet fluctuations; and (3) the inner shelf overdeepened sedimentary basins preserve an ultra

F1. Location map of sites drilled during ODP Leg 178, p. 13.



high resolution paleoceanographic record since the last glacial maximum, at least (Barker, Camerlenghi, Acton, et al., 1999).

A drastic change in seismic unit geometry and internal configuration identified on the continental shelf was postulated to indicate the transition from preglacial to glacial sedimentation on this part of West Antarctica. The most recent progradational and aggradational units developed above widespread unconformities and formed a sedimentary wedge with extraordinarily steep continental slope were believed to represent the glacial evolution of the margin (Units S1 and S2 in Fig. F2) (Larter and Barker, 1991; Larter et al., 1997). The underlying lens-shaped Unit S3, downlapping on a preexisting erosional surface, displaying subparallel reflectors, moderate divergence, and overall aggradational pattern, was instead believed to represent preglacial conditions.

Drilling at Sites 1097 and 1103 revealed instead that most of Unit S3 (the base of S3 was not reached by drilling) is composed of glaciogenic sediments (Shipboard Scientific Party, 1999b, 1999c). This finding allows us to relocate at deeper stratigraphic levels the so-called “onset of glaciation” on the northern Antarctic Peninsula. An effort to understand sedimentological and glaciological causes of such a different aspect between glacial Units S3 and overlying S1/S2 and to confine in time Unit S3 as accurately as possible with the available information obtained by drilling has been triggered by this finding. The age control of S3 is dependent, with a high degree of uncertainty, on biostratigraphy (Shipboard Scientific Party, 1999a) and strontium isotopic ratios of barnacles at one level of Site 1103 (Lavelle et al., Chap. 27, this volume), which both place S3 in the late Miocene.

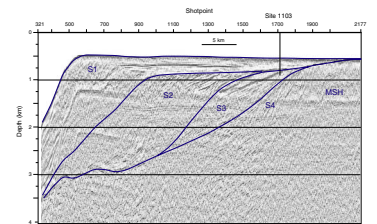
In this chapter, we present in detail an attempt to obtain ^{40}Ar - ^{39}Ar ages from volcanic clasts identified in the matrix of diamictites drilled within Unit S3 at Sites 1097 and 1103. These fragments were detected in generally low percentages as “volcanic glass” via smear slide description on board the *JOIDES Resolution*. Under normal conditions such grains would not attract interest for isotopic dating. However, we hypothesized that concentrations of volcanic grains resembling glass in the matrix of subglacial or ice-proximal diamictites could represent volcanic activity contemporaneous to deposition at the ice front or near-contemporaneous to erosion, transport, and deposition if the eruption happened on the continent just prior to the ice sheet advance on the continental shelf. We will show that in spite of analytical difficulties, volcanic clasts not necessarily concentrated in ash layers can provide an additional tool for chronostratigraphic reconstruction in glaciogenic sediments from the Antarctic margin.

SAMPLE PREPARATION AND DESCRIPTION

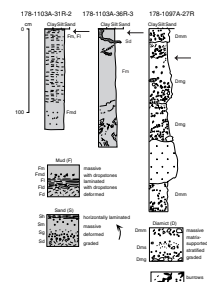
The geologic formations drilled through Unit S3 at Sites 1097 and 1103 are composed mainly of massive clast-rich diamict. At Site 1103, stratified diamicts, sandstones, and siltstone indicate deposition on a glacially influenced slope. At Site 1097, there is a wider range of sedimentary environments from subglacial deformation till to proglacial sediment gravity flow to open marine deposition (Fig. F3). Recovery was generally poor.

Following the smear slide descriptions provided by shipboard sedimentologists (Shipboard Scientific Party, 1999b, 1999c), we reexamined the diamict matrix at 10 locations that had volcanic glass contents re-

F2. Depth-converted multichannel seismic reflection profile, p. 14.



F3. Lithofacies of core sections, p. 15.

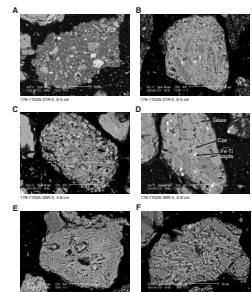


ported above 5%. With the exception of a single sample at Site 1097 that contains up to 75%–80% volcanic glass, all other samples contain 5% to 10% glass by visual estimation in smear slides. All samples were soaked in water for several months in an attempt to soften the matrix before disaggregation. The disaggregation was then done by hand in a mortar, by gentle wet crushing after 2 min of ultrasonic bath. Size separation was done by wet and dry sieving at sizes >2 mm, 2 mm–210 μm, and 210–150, 150–75, and 75–63 μm. Not all the resulting samples were suitable for further treatment because of the difficulty in separating individual volcanic clasts and because often volcanic clasts resulted in too poor concentration. Finally, we selected three samples, 178-1097A-27R-1, 35–58 cm, 178-1103A-31R-2, 0–4 cm, and 178-1103A-36R-3, 4–8 cm, which were treated with a Frantz Isodynamic separator and heavy liquids to concentrate homogeneous grains. The highest concentration of homogeneous grains was obtained in the range of 100–150 μm for all samples. Petrographical investigation of concentrates mounted with epoxy resin was carried out using a Philips XL30 scanning electron microscope (SEM) operating at 20 kV equipped with an X-ray energy dispersive system (EDS) EDAX DX4. Glass analyses were carried out using a JEOL JX 8600 electron microprobe (EMP) fitted with four wavelength-dispersive spectrometers (accelerating voltage = 15 kV; sample current = 10 nA; and beam size = 5–10 μm). Natural standards were used for calibration.

SEM-EDS observations revealed that all three sample concentrates consist of mineral clasts (including quartz, plagioclase, minor alkali-feldspar, and rare clinopyroxene, amphibole, biotite, and epidote), unsorted mineral aggregates (Fig. F4A), and abundant fragments of volcanic rock groundmass. The latter range from ipocrystalline to microcrystalline rocks. Textures vary from hyalopilitic at Site 1103, with variable proportions of plagioclase and well-preserved glass (Fig. F4B, F4C, F4D), to “intergranular” at Site 1097, with plagioclase laths and unresolvable alteration products possibly replacing interstitial glass (Fig. F4E, F4F). Fresh glass was not recognized in the sample from Site 1097. Plagioclase from all three samples ranges in composition from andesine to labradorite. Minor clinopyroxene and Fe-Ti oxide microclites occur in some groundmass grains from Site 1103 (Fig. F4D). Individual clasts are subrounded to rounded. Because some rounded clasts include both volcanic groundmass and a fine-grained glaciogenic matrix (e.g., Fig. F4B), we infer that roundness is due to mechanical reworking.

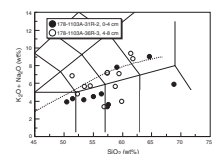
Table T1 lists the electron microprobe data on groundmass glass of samples from Site 1103. Most of the analyzed glasses fall in the subalkaline field of a total alkali vs. silica diagram (Fig. F5), some of them at the boundary between the subalkaline and alkaline and a few in the alkaline field. They range compositionally from trachybasalt to trachyte and from basalt to dacite (Fig. F5). Present data do not allow a clear definition of their affinity (i.e., orogenic vs. anorogenic). However, the relatively high TiO₂ and P₂O₅ contents (Table T1) point to a mature arc and/or to an anorogenic setting for some grains. The Ca/K ratio is variable and largely overlaps in the two samples (Table T1). It shows a negative correlation with SiO₂. The Cl content is relatively high (generally higher than 0.05 wt%). Cl/K ratios range from 0.033 to 0.095 in Sample 178-1103-36R-3, 4–8 cm, and from <0.008 to 0.12 in Sample 178-1103-31R-2, 0–4 cm (Table T1).

F4. Backscattered electron photomicrographs of grains mounted with epoxy resin, p. 16.



T1. Electron microprobe data on groundmass glasses, p. 23.

F5. Total alkali vs. silica classification diagram, p. 17.



⁴⁰Ar-³⁹Ar DATA

Analytical Procedures

Volcanic rock grains with a brownish to blackish appearance and rounded shapes were carefully concentrated by hand-picking under a binocular microscope, cleaned ultrasonically, and dried with pure acetone. The concentrates were wrapped in aluminium foil and irradiated in the TRIGA reactor at the University of Pavia (Italy) for 8 hr along with the biotite standard FCT-3 with an age of 27.95 Ma (Baksi et al., 1996). Values of the irradiation parameter J for individual sample packages were calculated by parabolic interpolation between the analyzed standards. Estimated uncertainty (one standard deviation) is 0.3%. Sample separation and argon step-heating experiments were carried out at the IGGI-CNR laboratory (Pisa). Because of the small grain size of volcanic fragments, they were not suitable for single-grain total fusion analyses. After irradiation, milligram-sized fractions (only for Samples 178-1097A-27R-1, 35–58 cm, and 178-1103A-36R-3, 4–8 cm) were spread on the bottom of 7-mm-diameter holes of a copper holder placed into a ultra high vacuum laser port and baked overnight at ~200°C. The samples were incrementally heated by a multimode laser beam generated by a continuous Nd:YAG (Nd-doped yttrium-aluminum-garnet) laser defocused to ~3-mm spot, and homogeneous heating was obtained by slowly rastering the laser beam (at 0.2 mm/s) by a computer-controlled x-y stage. In addition, with the aim of resolving as much as possible the true sample heterogeneity, various small fractions from the same irradiation packages of all three samples, each consisting of 10 grains for Sample 178-1097A-27R-1, 35–58 cm, and 30 grains for Samples 178-1103A-31R-2, 0–4 cm, and 36R-3, 4–8 cm, were incrementally laser heated over three steps. Gases extracted, gettered for 15 min (including about 5 min of lasering) for the milligram-sized samples and 10 min for the small fractions (including 1 min of lasering), were equilibrated via automated valves into a MAP215-50 noble gas mass spectrometer fitted with a Balzers SEV217 secondary electron multiplier. Argon isotope peak intensities were measured 10 times for a total time of ~20 min. Blanks were analyzed after every two to four runs. Data corrected for postirradiation decay, mass discrimination effects, isotopes derived from interfering neutron reactions, and blanks are listed in Tables T2 and T3. Errors are 2σ and do not include the uncertainty in the J value that was included in the total fusion ages. However, for analyses on small fractions the age errors are dominated by the experimental uncertainty. The most relevant correction factors used were as follows: $^{40}\text{Ar}/^{39}\text{Ar}_{(\text{K})} = 0.0096$, $^{36}\text{Ar}/^{37}\text{Ar}_{(\text{Ca})} = 0.00024$, and $^{39}\text{Ar}/^{37}\text{Ar}_{(\text{Ca})} = 0.00075$. Raw data reduction and age calculations were made using the program ArArCALC (v.2.0) (see Koppers, 1998).

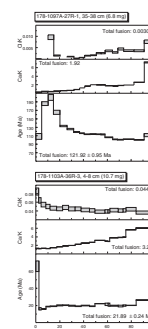
Results

Figure F6 shows the age spectra and Ca/K and Cl/K variations for the milligram-sized fractions of Samples 178-1097A-27R-1, 35–58 cm, and 178-1103A-36R-3, 4–8 cm; data are listed in Table T2. Both samples display irregularly discordant apparent age profiles. Sample 178-1097A-27R-1, 35–58 cm, after a first step at ~110 Ma, shows high apparent ages up to ~200 Ma that progressively decline to a minimum segment at ~100 Ma, with a slightly older final step (114 Ma) (Table T2). The total

T2. ⁴⁰Ar-³⁹Ar data on milligram-sized fractions, p. 24.

T3. ⁴⁰Ar-³⁹Ar data on multigrain fractions, p. 25.

F6. Age release and Ca/K and Cl/K spectra, p. 18.



fusion age is 122.1 ± 1.0 Ma. Sample 178-1103A-36R-3, 4–8 cm, exhibits a different apparent age pattern and significantly younger dates, characterized by high age in the first step (66 Ma) followed by a steady increase from 16 to 27 Ma. The total fusion age is 22.15 ± 0.24 Ma. For both samples, the Ca/K ratio displays a monotonic increase starting from values significantly lower than the bulk data in the first steps (Table T2; Fig. F6). The Ca/K ratios largely overlap in the two samples but, in Sample 178-1097A-27R-1, 35–58 cm, we observe a larger range (0.27–7.3 against 1.3–6.1) and significantly lower values in the low temperature steps. In Sample 178-1103A-36R-3, 4–8 cm, the Cl/K ratio shows a steady decline from 0.086 to 0.038 with increasing temperature, whereas in Sample 178-1097A-27R-1, 35–58 cm, it displays an irregular pattern in the first steps followed by a steady increase from the 0.35-W step. It is worthy of note that Sample 178-1103A-36R-3, 4–8 cm, Cl/K ratios show narrow variation and significantly higher values (~10 times higher) when compared to Sample 178-1097A-27R-1, 35–58 cm.

Figure F7 illustrates the age spectra and Ca/K variations of the step-heating experiments on the small fractions, and data are listed in Table T3. Most of the spectra display discordant apparent ages for the three steps. The use of small fractions strongly enhances the heterogeneity in age as observed in the milligram-sized fractions. Both samples exhibit a younger lower limit: 75 and 7.6 Ma for Samples 178-1097A-27R-1, 35–58 cm, and 178-1103A-36R-3, 4–8 cm, respectively. By contrast, the Ca/K ratios largely overlap with the ranges obtained from incremental heating of the milligram-sized fractions. Sample 178-1103A-31R-2, 0–4 cm, which was only analyzed as small fractions, shows a younger apparent age range (18–57 Ma) than the sample from Site 1097 (75–173 Ma) but older than the other sample from Site 1103 (7.6–50 Ma). The Cl/K ratios are higher than the sample from Site 1097 but similar to those of Sample 178-1103A-36R-3, 4–8 cm. It is to be noted that in Sample 178-1097A-27R-1, 35–58 cm, all the small fractions analyzed are characterized by marked increase in the Ca/K ratios from the first (with Ca/K \ll 1) to the last step. By contrast, both samples from Site 1103 commonly display a narrower variation (starting from values generally \gg 1). Note that in most instances the second and the third steps of both samples from Site 1103 have Ca/K ratios that overlap within errors (Fig. F7).

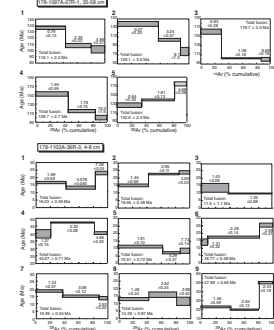
DISCUSSION

Interpretation of Argon Data

When interpreting the present results, one should bear in mind that the data, particularly for the small fractions, derive from mixtures of volcanic groundmass with different chemical compositions and, potentially, eruption ages. Indeed, the Antarctic Peninsula area experienced a complex Mesozoic and Cenozoic plate tectonic evolution that was accompanied by igneous activity with different geochemical signatures. Glaciogenic sediments are therefore expected to reflect the complex igneous activity that affected the area in time. An important observation is that volcanic grains show evidence for abrasion resulting from mechanical reworking. This implies that age constraints derived from these samples should be taken as the oldest limit for their deposition.

On the other hand, disturbed age spectra are common even for argon data extracted from a single specimen. Groundmass samples are poly-mineralic mixtures that may also include glass; each component may

F7. Age release spectra of small fractions, p. 19.



retain a distinct argon signature as a function of secondary alteration processes and potential analytical artifacts. Discordant age spectra may therefore arise from a complex interplay of secondary alteration processes (producing ⁴⁰Ar* loss and/or potassium addition) and possibly from analytical artifacts resulting from the common fine grain size of primary and secondary minerals within the groundmass. Very fine grained mineral phases may experience argon isotope redistribution and/or loss during irradiation because of recoil processes. Discordant ⁴⁰Ar-³⁹Ar age spectra can occur because the argon step-heating technique, because of the differential thermal stability of mineral phases during in-vacuo heating, has the potential to separate different argon reservoirs hosted in different mineralogical domains. The contribution of each different mineral phase to the age spectra, however, may be monitored by elemental variations (Ca, Cl, and K from neutron-derived ³⁷Ar, ³⁸Ar, and ³⁹Ar, respectively). Meaningful interpretation of groundmass argon data, therefore, requires the support of petrographical and chemical analyses at a microscopic scale. As an example, Lo et al. (1994) and Koppers et al. (2000) have shown that argon step-heating analyses on volcanic rocks commonly exhibit low apparent Ca/K ratios and high meaningless apparent ages in the low-temperature region. This feature derives from the lower release temperature of K-rich alteration mineral phases that may experience ³⁹Ar recoil loss during irradiation. Koppers et al. (2000) also observed low meaningless apparent ages in high-temperature steps that, based on the concomitant increase of the Ca/K ratios, was attributed to preferential degassing at the high temperature of plagioclase and clinopyroxene affected by ³⁷Ar recoil loss. Lo et al. (1994) instead observed high meaningless apparent ages in the high-temperature steps. This was related to the release of argon from phenocrysts that may host extraneous argon (both inherited or excess argon). However, the intermediate region of the age spectra attributed to outgassing of glass and groundmass plagioclase by Lo et al. (1994) and of interstitials (glassy or microcrystalline) by Koppers et al. (2000) may yield meaningful ages. In general, volcanic glasses were dated with variable success. On one hand, both low and high meaningless ages were reported (e.g., Mankinen and Dalrymple, 1972; Walker and McDougall, 1982; Cerling et al., 1985). This is attributable to (1) hydration and devitrification and (2) incorporation of excess argon in quenched basaltic glass in the submarine environment (cf. McDougall and Harrison, 1988). On the other hand, other studies reported K-Ar or ⁴⁰Ar-³⁹Ar data on volcanic glass yielding internally consistent results (e.g., Sharp et al., 1996; Pinti et al., 2001) or concordant with coexisting alkali feldspar (e.g., Drake et al., 1980). Thus, the validation of a ⁴⁰Ar-³⁹Ar age derived from volcanic glass requires the support of independent evidence or of different geochronological data.

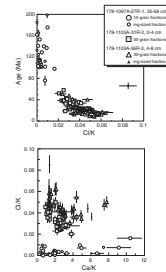
Examination of the incremental heating analyses on milligram-sized fractions (Table T2) reveals that the sample from Site 1097 is characterized by a significant fraction of gas (37% of ³⁹Ar released) with Ca/K ratios $\ll 1$, whereas, in spite of the extended low-temperature heating schedule, no Ca/K ratios < 1 were detected in the samples from Site 1103. This, in agreement with SEM-EDS observation, reflects the higher alteration degree of the sample from Site 1097 than the samples from Site 1103. It is worthy of note that the final steps of the milligram-sized and small fractions for all samples do not show high Ca/K ratios attributable to a significant contribution from pyroxene (Ca/K > 300 in the study samples). Most of the Ca/K ratios derived from argon data for

samples from Site 1103 are compatible with outgassing of groundmass glass with possible contamination by groundmass plagioclase ($\text{Ca}/\text{K} > 16$, based on EDS analyses). Nevertheless, Cl/K ratios derived from argon data show a narrower variation than electron microprobe analyses (0.024–0.061 vs. 0.033–0.095 and 0.021–0.048 vs. ≤ 0.008 –0.12 for Sample 176-1103A-36R-3, 4–8 cm, and 31R-2, 0–4 cm, respectively) (Tables T1, T3). The meaning of such disagreement remains uncertain. When comparing argon data with EMP analyses, one should bear in mind that the latter refer to single-grain analysis. By contrast, argon analyses investigated a volumetrically much larger sample, which may approach the true average of the whole population.

Figure F8 shows three-isotope correlation plots whose argon isotope ratios have been converted to age and elemental ratios. The distribution of data points in Figure F8 is compatible for the three samples with multicomponent systems. It is interesting to note that, based on different recoil lengths of argon isotopes (i.e., $^{37}\text{Ar} > ^{39}\text{Ar} \gg ^{38}\text{Ar}$) (Onstott et al., 1995), it is likely to obtain during sample irradiation of very fine intergrowths (at least for intergrowths > 20 nm thick) significant displacement of ^{37}Ar and ^{39}Ar accompanied by an undetectable effect on ^{38}Ar . In Figure F8A this process would produce a distribution of data points along a trend with a positive slope, whereas it would have a less important effect on the Ca/K ratios. Whereas a similar process may explain the argon isotope compositions of the low-temperature region of the milligram-sized fraction of Sample 178-1097A-27R-1, 35–58 cm, and of the first step (age ~ 66 Ma) of the milligram-sized fraction of Sample 178-1103A-36R-3, 4–8 cm, it cannot explain (1) the distribution of the remaining steps of the milligram-sized fractions, (2) the argon isotope composition of the small fractions, and (3) the overall negative correlation of Figure F8B. The negative correlation between age and Cl/K , such that lower Cl/K analyses give higher ages, is the most striking feature of Figure F8. Based on the Ca, Cl, and K contents, the Cl/K variations correspond to differences in Cl. Given the imperfect agreement between argon data and electron microprobe analyses on glasses (see above) and the lack of Cl determinations on volcanic rocks of the area from literature, the question of whether the Cl variation reflects a true increase with decreasing age of the igneous activity or is an analytical artifact remains unclear and requires further investigation.

Following the interpretation that argon data from Site 1103 are derived mainly from volcanic glass and *assuming that analyzed glasses are free from K and Ar mobility*, we may speculate that the age intervals defined by the argon data of the small fractions (18–57 Ma for Sample 178-1103A-31R-2, 0–4 cm, and 7.6–50 Ma for Sample 178-1103A-36R-3, 4–8 cm) provide for each sample an estimate of the maximum youngest limit and the minimum oldest limit for the eruption age of the volcanic sequence sampled by the glacial erosion. Because for Sample 178-1097A-27R-1, 35–58 cm, fresh glass was not detected on epoxy-mounted grains, we believe that the age range of 75–173 Ma can be taken only as indicative of the age variation of the volcanic clasts recovered at 220 mbsf at Site 1097. This age interval vastly exceeds the plausible depositional age of sequence group S3. At Site 1103, the hypothesized maximum youngest limit for the volcanic activity as sampled by glacial erosion (7.6 ± 0.7 Ma) and detected close to the bottom of drilling (340 mbsf) is compatible with the age range of the diatom Zone *Actinocyclus ingens* v. *ovalis* (6.3–8.0 Ma) determined for the interval 320–355 mbsf at the same site (Shipboard Scientific Party, 1999c). In addition, it agrees with the maximum ages of 7.4 (+1.5/–0.9) and 7.8

F8. Three-isotope correlation diagrams, p. 21.

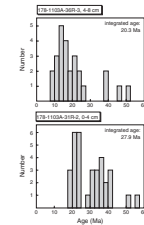


(+1.5/−1.1) Ma obtained at 262–263 mbsf from strontium isotope composition of barnacle fragments (Lavelle et al., [Chap. 27](#), this volume). With the above-mentioned assumptions concerning K and Ar mobility, the 7.6-Ma age provides an estimate for the maximum age of sequence group S3 at 340 mbsf, bearing in mind, in addition, that (1) the distribution of the age-steps (only two ages younger than 10 Ma of the 26 analyses) suggests the presence of grains with apparent ages younger than 7.6 Ma (Fig. F9) and (2) analyzed grains show evidence for abrasion supporting mechanical reworking. An additional point deserving attention is that from the distribution of the age steps of the small fractions at Site 1103 (Fig. F9) we note that with decreasing sample depth (340 and 290 mbsf for Samples 178-1103A-36R-3, 4–8 cm, and 31R-2, 0–4 cm, respectively), volcanic clasts show overall increasing apparent ages. This is compatible with glacial erosion that affected with time deeper levels of a volcanic sequence previously deposited on the continent. This observation is compatible with the interpretation of S3 as representing an initial stage of development of the glacial margin that preceded the dramatic advances of the ice sheet to the continental shelf edge represented by S1 and S2 (Barker et al., in press).

CONCLUSIONS

1. Three diamict matrix samples, recovered at Sites 1097 and 1103 (ODP Leg 178) within sequence group S3, contain variable proportions of fragments of volcanic rocks, mostly within the 100- to 150- μ m grain-size range. They are characterized by rounded to subrounded shapes that suggest mechanical reworking. Fresh glass was only recognized in grains from Site 1103.
2. ⁴⁰Ar-³⁹Ar incremental laser-heating experiments over three steps on numerous small fractions yielded ages of 75–173 Ma for Sample 178-1097A-27-1, 35–58 cm (220 mbsf); 18–57 Ma for Sample 178-1103A-31R-2, 0–4 cm (290 mbsf); and 7.6–50 Ma for Sample 178-1103A-36R-3, 4–8 cm (340 mbsf). Based on SEM-EDS and EMP investigations, the ages for samples from Site 1103 are mainly from groundmass glass. The youngest apparent age (7.6 Ma) for the volcanic activity detected at 340 mbsf, close to the bottom of Hole 1103A, is compatible with the age range of the diatom *Actinocyclus ingens* v. *ovalis* Zone (6.3–8.0 Ma) of the interval 320–355 mbsf at the same site (Shipboard Scientific Party, 1999c) and with the maximum ages derived from the strontium isotope composition of barnacle fragments (Lavelle et al., [Chap. 27](#), this volume). However, use of the ⁴⁰Ar-³⁹Ar data to constrain the age of Sequence S3 at 340 mbsf would require the support of further research.
3. The overall negative correlation between apparent ⁴⁰Ar-³⁹Ar ages and sample depth at Site 1103 is compatible with glacial erosion that affected with time deeper levels of a volcanic sequence previously deposited on the continent.
4. On the whole, the three samples show a negative correlation between apparent ages and Cl/K ratios. This is compatible with an increase of Cl content with decreasing age of volcanic activity.
5. Incremental laser-heating analyses over few steps on numerous small fractions may be used to place age constraints on mixed populations of volcanic glass-bearing groundmass clasts hosted in sediments. This is the only available means when the small

F9. Histograms of age, p. 22.



grain size (in this study as low as 100–150 μm) of homogenous grains and/or the low potassium contents do not allow single-grain laser fusion analyses. From a broad perspective, this approach (joined to single-grain major element analyses on glass by the electron microprobe and, possibly, trace element determinations by the laser ablation inductively coupled plasma–mass spectrometry [ICP-MS] technique [e.g., see Bryant et al., 1999]) appears to be useful in provenance studies. Alternatively, where volcanic sequences have been completely eroded, it may represent an additional tool in defining the temporal and compositional evolution of igneous activity in plate margin settings.

ACKNOWLEDGMENTS

We are grateful to G. Giorgetti and F. Olmi for support during SEM-EDS investigation at the Dipartimento di Scienze della Terra of Siena and EMP analyses at the Centro Studi per la Minerogenesi e la Geochimica Applicata, CNR, Firenze, respectively. We also thank G. Ferrara for discussing many aspects of this work. The manuscript was improved by careful review by P. Leat and W.C. McIntosh. The argon laserprobe facility was funded by the Programma Nazionale di Ricerche in Antartide (PNRA).

This research used samples and/or data provided by the Ocean Drilling Program (ODP). ODP is sponsored by the U.S. National Science Foundation (NSF) and participating countries under management of Joint Oceanographic Institutions (JOI), Inc. Funding for this research was provided by Consiglio Nazionale delle Ricerche and PNRA.

REFERENCES

- Baksi, A.K., Archibald, D.A., and Farrar, E., 1996. Intercalibration of ⁴⁰Ar/³⁹Ar dating standards. *Chem. Geol.*, 129:307–324.
- Barker, P.F., 1982. The Cenozoic subduction history of the Pacific margin of the Antarctic Peninsula: ridge crest-trench interactions. *J. Geol. Soc. London*, 139:787–801.
- Barker, P.F., and Camerlenghi, A., 1999. An approach to Antarctic glacial history: the aims of Leg 189. In Barker, P.F., Camerlenghi, A., Acton, G.D., et al., *Proc. ODP, Init. Repts.*, 178, 1–44 [CD-ROM]. Available from: Ocean Drilling Program, Texas A&M University, College Station, TX 77845-9547, U.S.A.
- Barker, P.F., Camerlenghi, A., Acton, G.D., et al., 1999. *Proc. ODP, Init. Repts.*, 178 [CD-ROM]. Available from: Ocean Drilling Program, Texas A&M University, College Station, TX 77845-9547, U.S.A.
- Barker, P.F., Camerlenghi, A., and the ODP Leg 178 Shipboard Scientific Party, in press. Antarctic glacial history, step 1: the continental margin drilled by ODP Leg 178. *N. Z. J. Geol. Geophys.*
- Bryant, C.J., Arculus, R.J., and Eggins, S.M., 1999. Laser ablation-inductively coupled plasma-mass spectrometry and tephras: a new approach to understanding arc-magma genesis. *Geology*, 27:1119–1122.
- Camerlenghi, A., Rebesco, M., De Santis, L., and Volpi, V., in press. The Antarctic Peninsula Pacific Margin: modelling flexure and decompaction with constraints from ODP Leg 178 initial results. *N. Z. J. Geol. Geophys.*
- Cerling, T.E., Brown, F.H., and Bowman, J.R., 1985. Low-temperature alteration of volcanic glass: hydration, Na, K, ¹⁸O and Ar mobility. *Chem. Geol.*, 52:281–293.
- Drake, R.E., Curtis, G.H., Cerling, T.E., Cerling, B.W., and Hampel, J., 1980. KBS Tuff dating and geochronology of tuffaceous sediments in Koobi Fora and Shungura formations, East Africa. *Nature*, 283:368–372.
- Hole, M.J., 1990. Geochemical evolution of Pliocene-Recent post-subduction alkalic basalts from Seal Nunataks, Antarctic Peninsula. *J. Volcanol. Geotherm. Res.*, 40:149–167.
- Irvine, T.N., and Baragar, W.R.A., 1971. A guide to the chemical classification of the common volcanic rocks. *Can. J. Earth Sci.*, 8:523–548.
- Koppers, A.A.P., 1998. ⁴⁰Ar/³⁹Ar geochronology and isotope geochemistry of the West Pacific seamount province: implications for absolute Pacific plate motion and the motion of hot spots [Ph.D. dissert.]. Vrije Universiteit Amsterdam, The Netherlands.
- Koppers, A.A.P., Staudigel, H., and Wijbrans, J.R., 2000. Dating crystalline groundmass separates of altered Cretaceous seamount basalts by the ⁴⁰Ar/³⁹Ar incremental heating technique. *Chem. Geol.*, 166:139–158.
- Larter, R.D., and Barker, P.F., 1991. Neogene interaction of tectonic and glacial processes at the Pacific margin of the Antarctic Peninsula. In Macdonald, D.I.M. (Ed.), *Sedimentation, Tectonics and Eustasy: Sea-level Changes at Active Margins*. Spec. Publ. Int. Assoc. Sedimentol., 12:165–186.
- Larter, R.D., Rebesco, M., Vanneste, L.E., Gamboa, L.A.P., and Barker, P., 1997. Cenozoic tectonic, sedimentary and glacial history of the continental shelf west of Graham Land, Antarctic Peninsula. In Cooper, A.K., Barker, P.F., and Brancolini, G. (Eds.), *Geology and Seismic Stratigraphy of the Antarctic Margin* (Pt. 2). *Antarct. Res. Ser.*, 71:1–27.
- Le Bas, M.J., Le Maitre, R.W., Streckeisen, A., and Zanettin, B.A., 1986. Chemical classification of volcanic rocks based on the total alkali-silica diagram. *J. Petrol.*, 27:745–750.
- Lo, C.-H., Onstott, T.C., Chen, C.-H., and Lee, T., 1994. An assessment of ⁴⁰Ar/³⁹Ar dating for the whole-rock volcanic samples from the Luzon Arc near Taiwan. *Chem. Geol.*, 114:157–178.

- Mankinen, E.D., and Darlymple, G.B., 1972. Electron microprobe evaluation of terrestrial basalts for whole-rock dating. *Earth Planet. Sci. Lett.*, 17:89–94.
- McDougall, I., and Harrison, T.M., 1988. *Geochronology and Thermochronology by the ⁴⁰Ar/³⁹Ar Method*: New York (Oxford Univ. Press).
- Onstott, T.C., Miller, M.L., Ewing, R.C., Arnold, G.W., and Walsh, D.S., 1995. Recoil refinements: implications for the ⁴⁰Ar/³⁹Ar dating technique. *Geochim. Cosmochim. Acta*, 59:1821–1834.
- Pinti, D.L., Quidelleur, X., Chiesa, S., Ravazzi, C., and Gillot, P.Y., 2001. K-Ar dating of an early middle Pleistocene distal tephra in the interglacial varved succession of Piànico-Sèllere (Southern Alps, Italy). *Earth Planet. Sci. Lett.*, 188:1–7.
- Rebesco, M., Camerlenghi, A., and Zanolla, C., 1998. Bathymetry and morphogenesis of the continental margin west of the Antarctic Peninsula. *Terra Antart.*, 5:715–728.
- Sharp, W.D., Turrin, B.D., Renne, P.R., and Lanphere, M.A., 1996. The ⁴⁰Ar/³⁹Ar and K/Ar dating of lavas from the Hilo 1-km hole, Hawaii Scientific Drilling Project. *J. Geophys. Res.*, 101(B5):11,607–11,616.
- Shipboard Scientific Party, 1999a. Leg 178 summary: Antarctic glacial history and sea-level change. In Barker, P.F., Camerlenghi, A., Acton, G.D., et al., *Proc. ODP, Init. Repts.*, 178, 1–83 [CD-ROM]. Available from: Ocean Drilling Program, Texas A&M University, College Station, TX 77845-9547, U.S.A.
- , 1999b. Site 1097. In Barker, P.F., Camerlenghi, A., Acton, G.D., et al., *Proc. ODP, Init. Repts.*, 178, 1–66 [CD-ROM]. Available from: Ocean Drilling Program, Texas A&M University, College Station, TX 77845-9547, U.S.A.
- , 1999c. Shelf Transect (Sites 1100, 1102, and 1103). In Barker, P.F., Camerlenghi, A., Acton, G.D., et al., *Proc. ODP, Init. Repts.*, 178, 1–83 [CD-ROM]. Available from: Ocean Drilling Program, Texas A&M University, College Station, TX 77845-9547, U.S.A.
- Smellie, J.L., 1999. Lithostratigraphy of Miocene-Recent alkaline volcanic fields in the Antarctic Peninsula and eastern Ellsworth Land. *Antarct. Sci.*, 11:362–378.
- Walker, D.A., and McDougall, I., 1982. ⁴⁰Ar/³⁹Ar and K-Ar dating of altered glassy volcanic rocks: the Dabi Volcanics. *Geochim. Cosmochim. Acta*, 46:2181–2190.

Figure F1. Location map of sites drilled during ODP Leg 178. Sites 1097 and 1103 were drilled on the continental shelf. Bathymetry is after Rebesco et al. (1998).

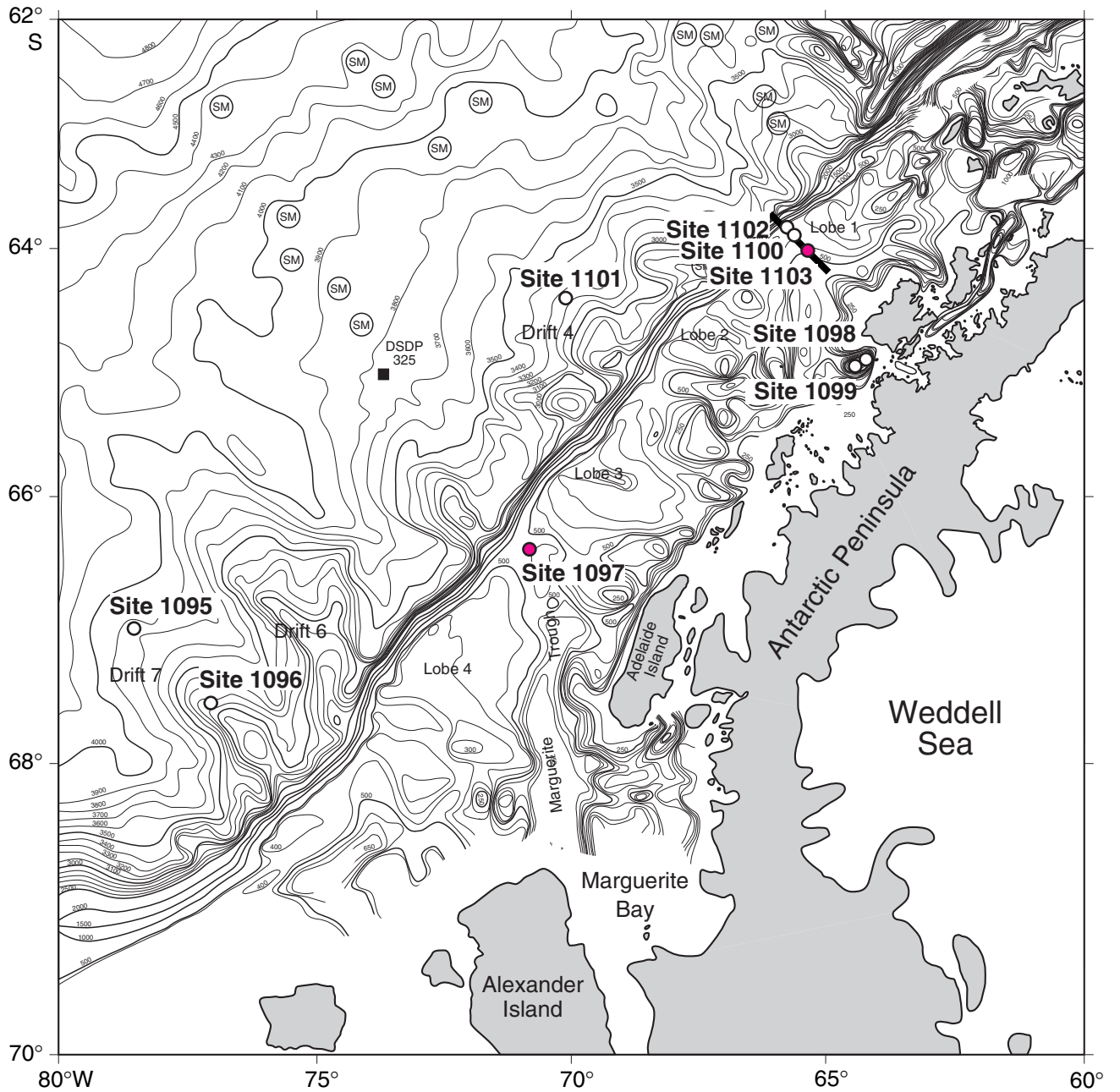


Figure F2. Depth-converted multichannel seismic reflection profile I95–152 (modified after Camerlenghi et al., in press), showing the different geometry between Units S1/S2 and S3 (see “**Introduction**,” p. 2, for details). Unit S4 is believed to be older than the tectonic uplift of the margin. MSH = mid-shelf high, as described in Larter and Barker (1991).

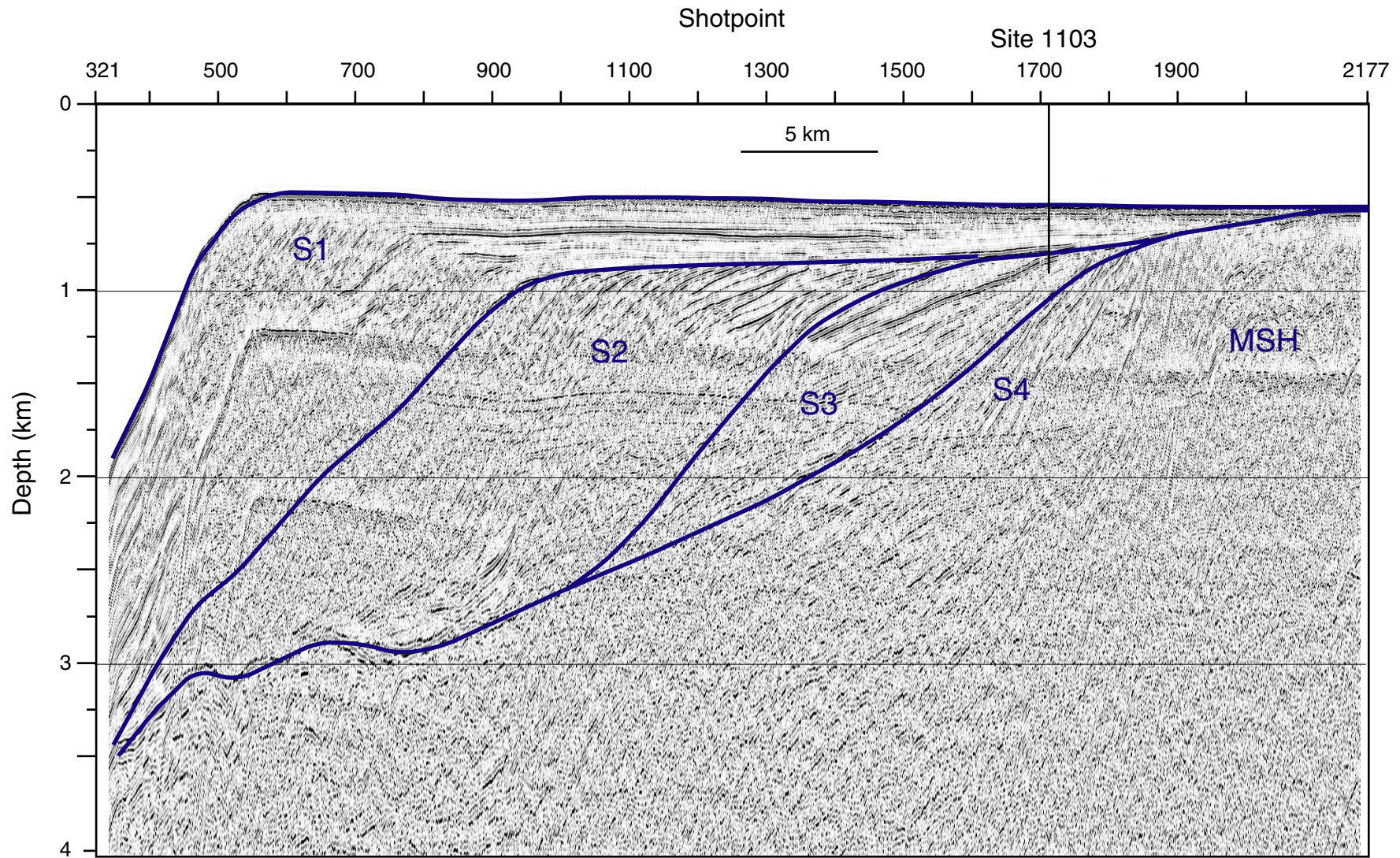


Figure F3. Lithofacies of core sections selected for this study within seismic Unit S3 (modified after Shipboard Scientific Party, 1999b, 1999c). Arrows indicate location of samples. All lithofacies represent indurated sediments.

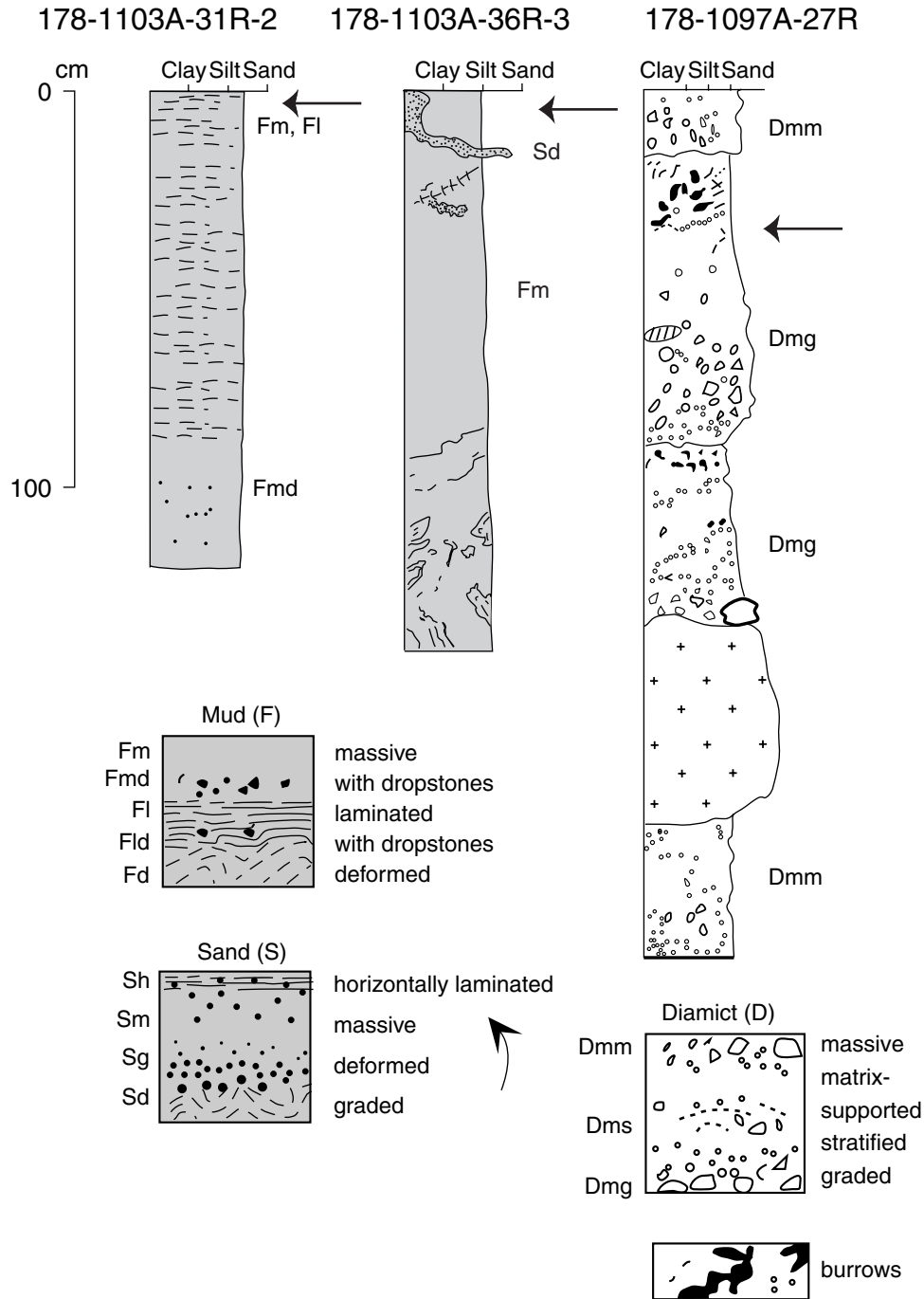


Figure F4. Backscattered electron photomicrographs of grains mounted with epoxy resin. (A) Diamicrite and (B) volcanic groundmass grain consisting of plagioclase laths and Fe-Ti oxides enclosed in glass (Sample 178-1103A-31R-2, 0–4 cm). (C) Volcanic groundmass grain consisting of plagioclase laths and Fe-Ti oxides enclosed in glass and (D) the same matrix but with a different proportion of plagioclase(Pl)-glass and minor clinopyroxene (Cpx) (Sample 178-1103A-36R-3, 4–8 cm). (E, F) Grains consisting of plagioclase and irresolvable alteration products probably replacing interstitial glass (Sample 178-1097A-27R-1, 38–58 cm). Note that volcanic groundmass grains of the three samples show rounded shapes resulting from mechanical reworking.

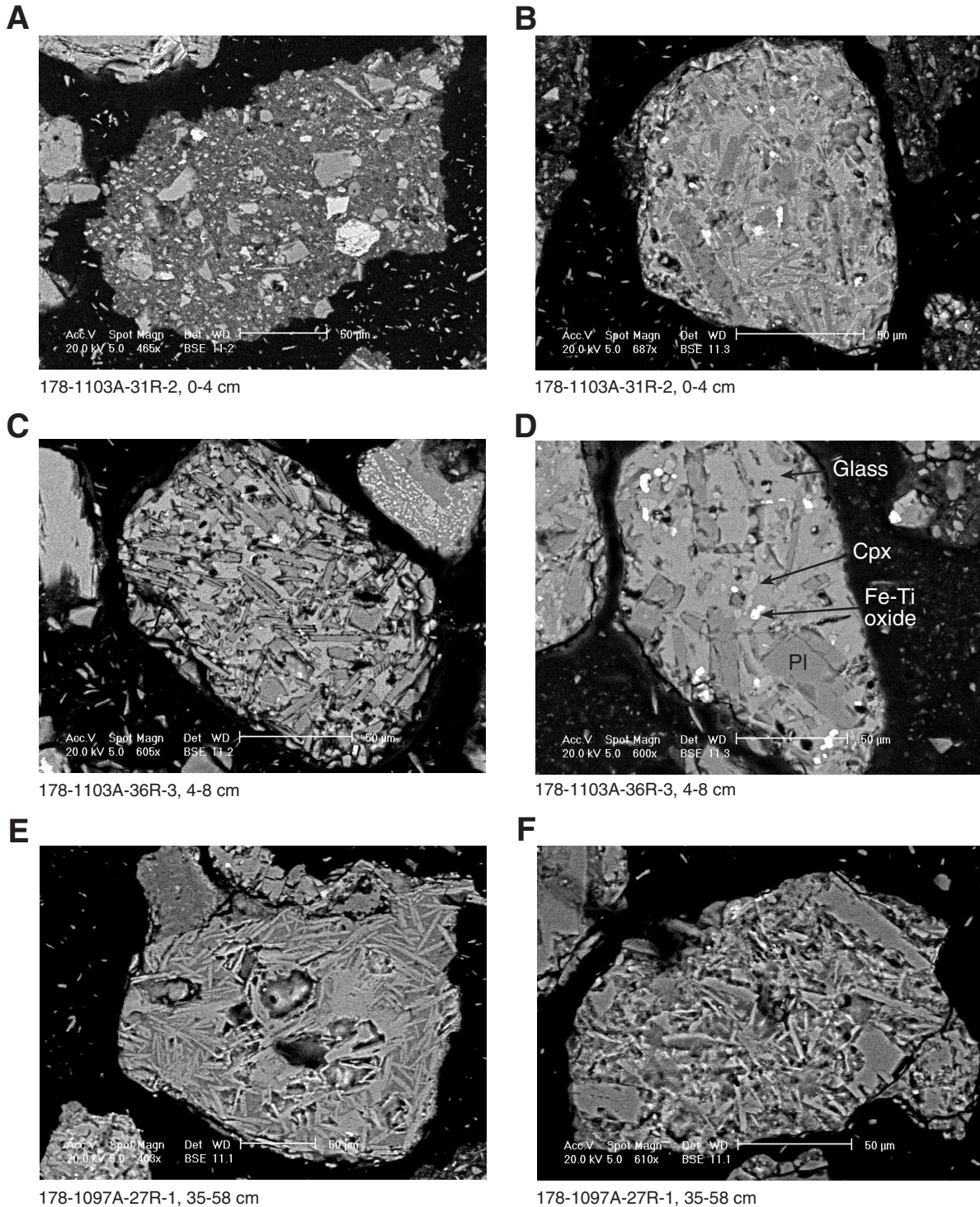


Figure F5. Total alkali vs. silica classification diagram (LeBas et al., 1986) of the analyzed glasses from Site 1103. The discriminating curve of alkaline and subalkaline field is from Irvine and Baragar (1971).

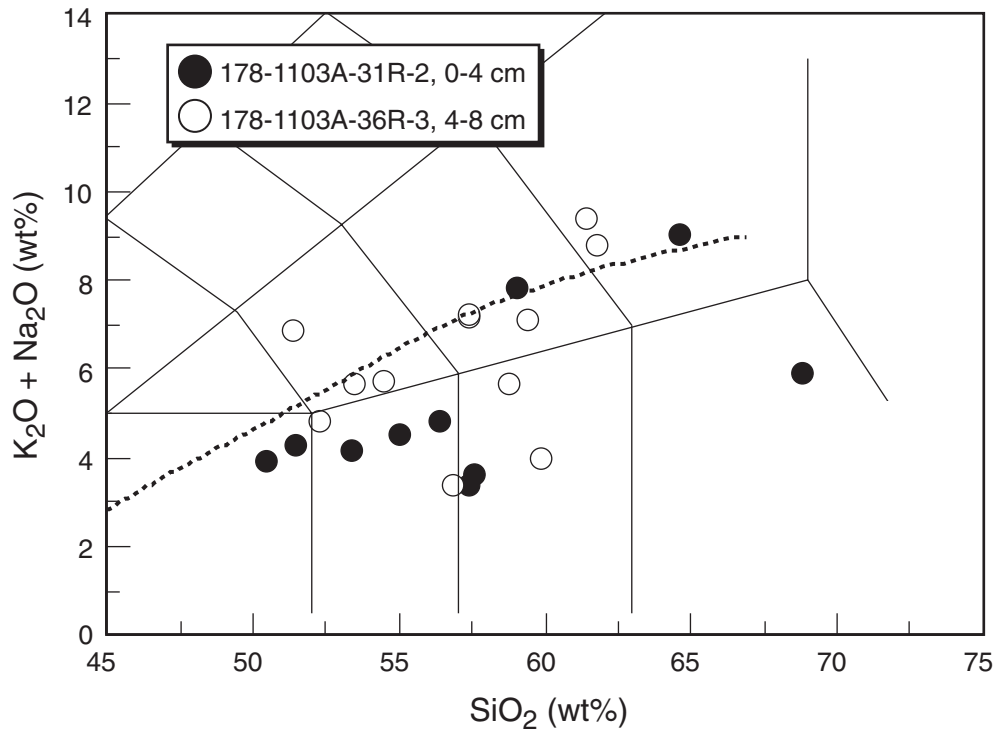


Figure F6. Age release and Ca/K and Cl/K spectra of the milligram-sized fraction from Samples 178-1097A-37R-1, 35–38 cm, and 178-1103A-36R-3, 4–8 cm. Errors are 2 σ .

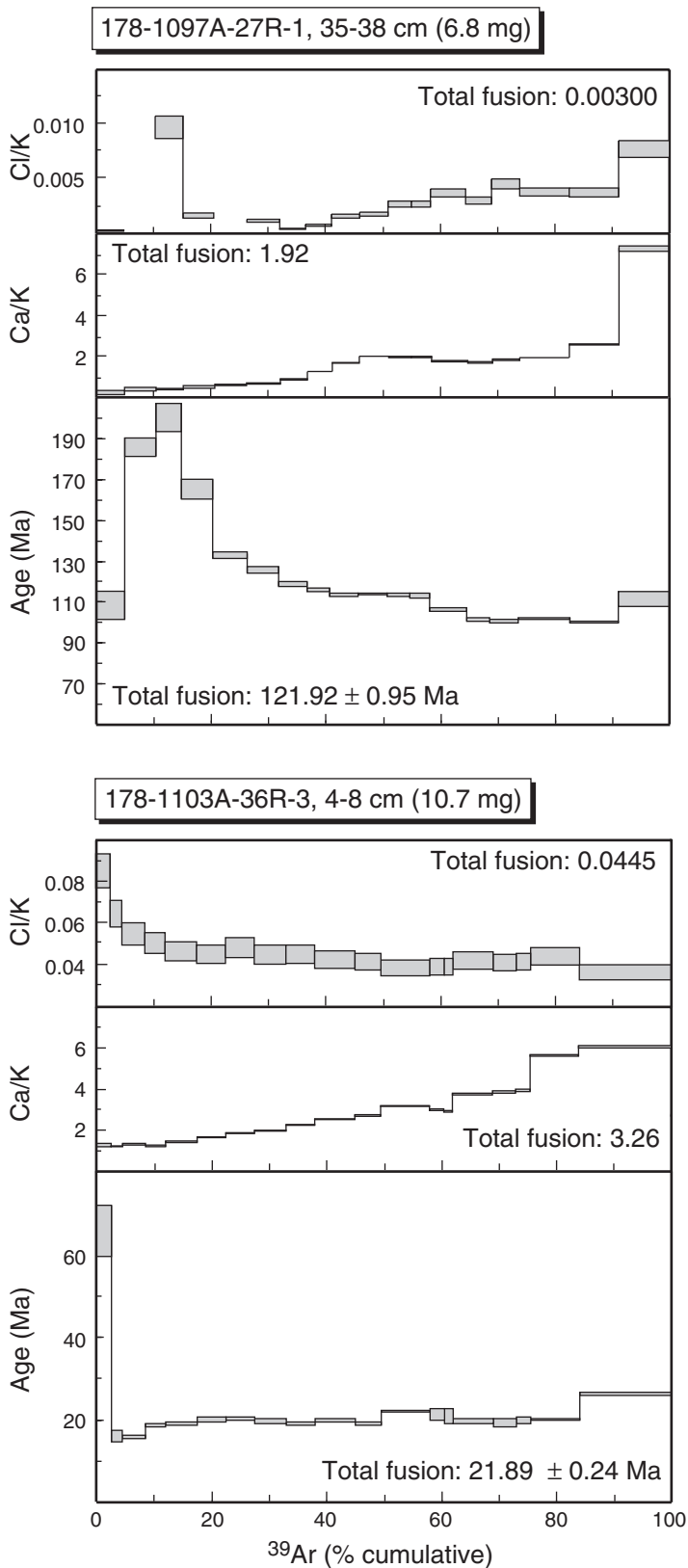


Figure F7. Age release spectra of small fractions (10 grains for the Site 1097; 30 grains for Site 1103). Numbers reported for each age step refer to the Ca/K ratios. Errors are 2 σ . (Continued on next page.)

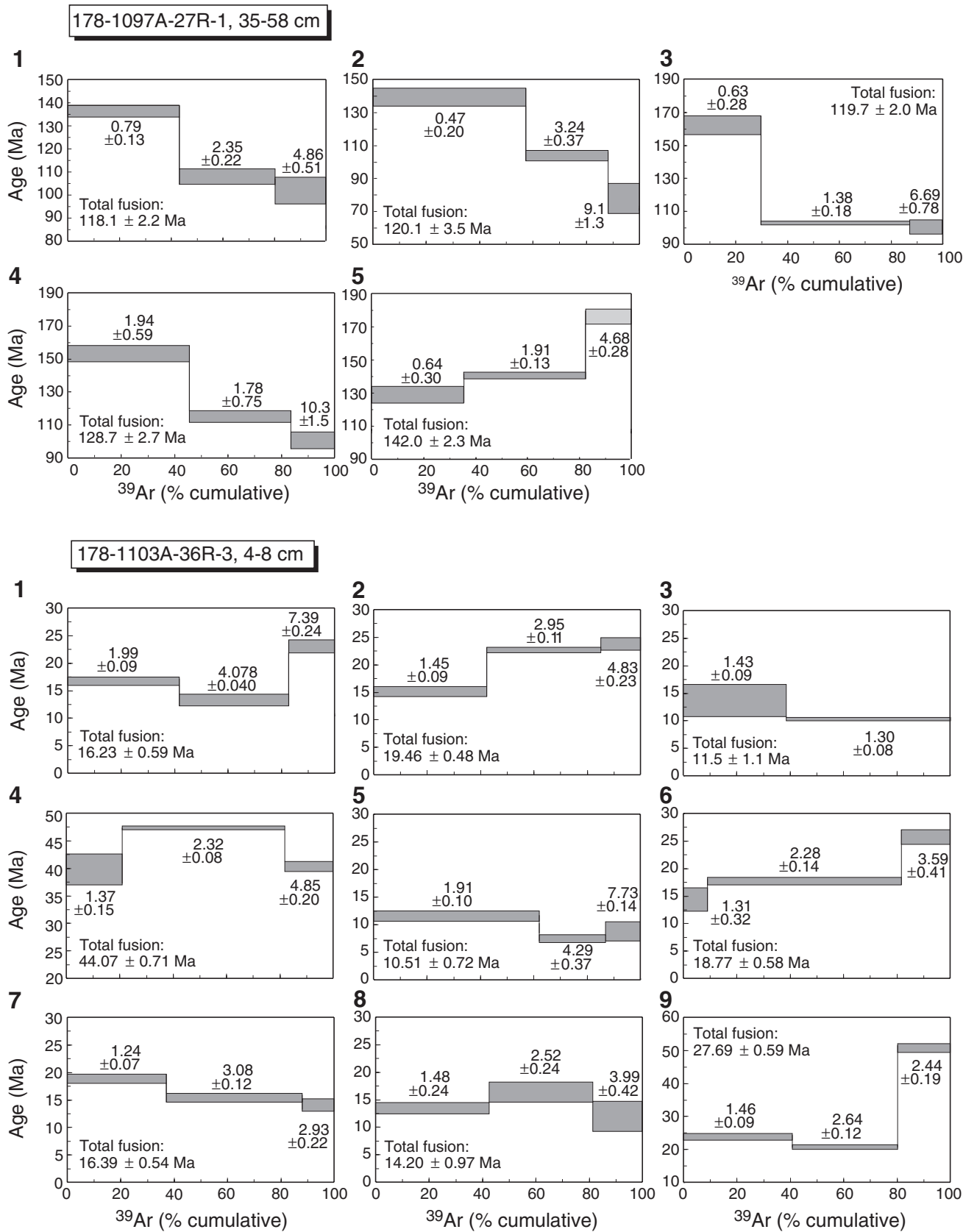


Figure F7 (continued).

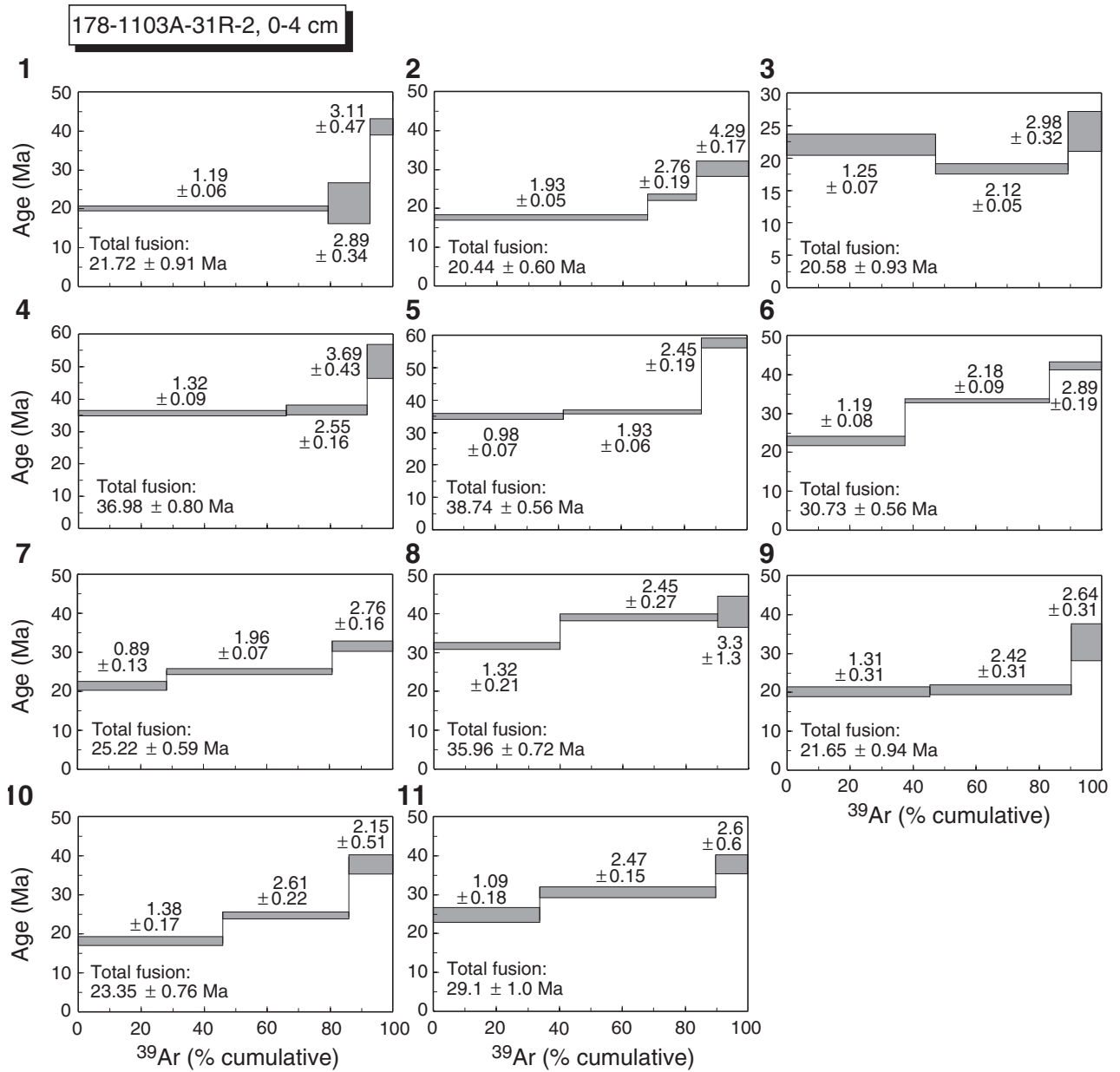


Figure F8. Three-isotope correlation diagrams (argon isotope ratios converted to age and elemental ratios) for argon data of the three samples. Errors are 2σ .

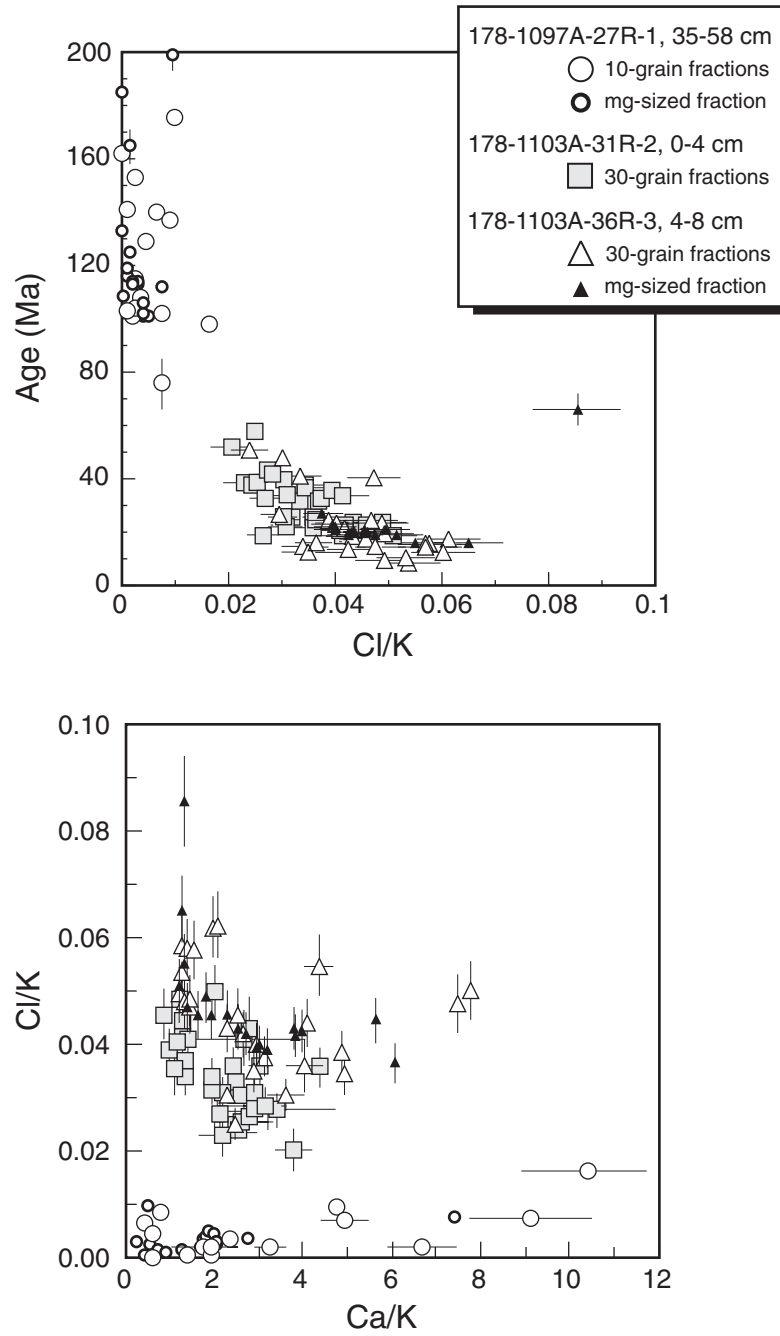


Figure F9. Histograms of age in small fractions of the samples from Site 1103.

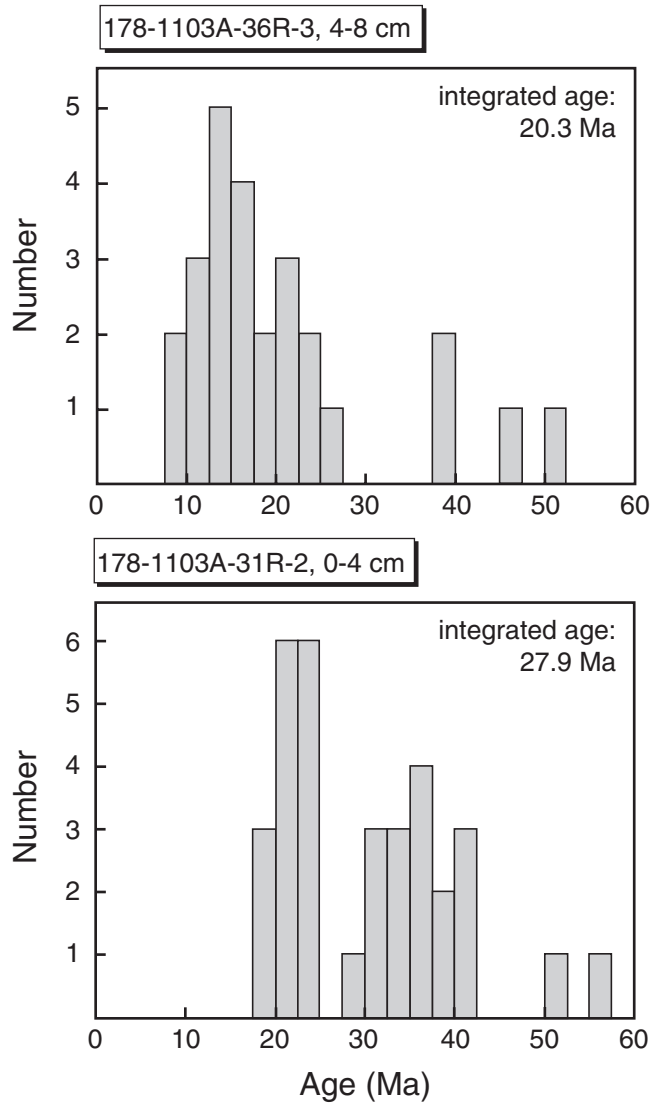


Table T1. Electron microprobe data on groundmass glasses, Site 1103.

	1	2	3	4	5	6	7	8	9	10	11	12
178-1103A-36R-3, 4–8 cm												
SiO ₂	56.18	52.18	57.78	57.34	55.09	51.71	50.73	54.29	56.34	61.10	60.01	57.31
TiO ₂	2.14	2.40	2.08	2.24	2.12	1.83	1.80	2.21	2.79	1.84	1.84	2.38
Al ₂ O ₃	13.13	13.32	13.70	15.20	14.72	14.57	14.70	13.96	12.99	14.31	14.24	13.76
FeO	13.16	12.56	10.65	8.31	8.36	10.30	11.55	11.79	10.22	7.06	7.05	8.75
MnO	0.26	0.27	0.27	0.21	0.12	0.22	0.29	0.19	0.20	0.25	0.12	0.19
MgO	3.51	3.21	2.38	2.61	2.61	5.22	4.07	3.70	2.51	1.38	1.59	2.05
CaO	6.62	7.18	4.99	5.31	5.39	9.86	8.44	7.22	5.25	2.84	2.79	4.33
Na ₂ O	1.78	2.95	1.74	2.44	3.71	3.46	4.77	3.89	2.98	5.25	3.31	3.62
K ₂ O	1.54	2.61	2.13	3.08	3.22	1.31	2.03	1.80	4.06	4.10	5.25	3.21
F	BDL	BDL	BDL	0.07	BDL	BDL	BDL	0.08	BDL	0.50	0.11	BDL
Cl	0.11	0.08	0.13	0.08	0.08	0.09	0.10	0.07	0.13	0.15	0.15	0.10
P ₂ O ₅	0.44	0.87	0.72	0.66	0.52	0.38	0.29	0.41	0.73	0.69	0.66	0.74
Total	98.87	97.63	96.57	97.55	95.94	98.95	98.77	99.61	98.2	99.47	97.12	96.44
Ca/K	3.61	2.31	1.97	1.45	1.41	6.32	3.49	3.37	1.09	0.58	0.45	1.13
Cl/K	0.095	0.041	0.081	0.035	0.033	0.091	0.065	0.052	0.043	0.049	0.038	0.041
178-1103A-31R-2, 0–4 cm												
SiO ₂	55.60	54.08	55.35	50.12	53.16	55.33	66.77	51.57	56.94	63.91		
TiO ₂	2.14	2.53	1.76	2.20	1.96	2.17	1.73	2.32	2.14	1.36		
Al ₂ O ₃	14.38	14.62	14.74	14.56	13.25	14.10	14.37	13.76	14.56	17.39		
FeO _{Tot}	11.25	10.52	10.74	12.08	13.01	11.23	5.72	12.98	7.49	2.69		
MnO	0.29	0.25	0.24	0.26	0.17	0.26	0.13	0.28	0.20	0.13		
MgO	2.89	3.77	3.16	5.34	4.48	2.90	0.53	5.16	2.00	0.51		
CaO	6.17	7.50	6.81	10.57	8.93	6.24	1.97	9.40	4.27	3.21		
Na ₂ O	1.79	2.81	2.96	2.97	2.66	1.93	2.35	2.69	3.86	5.09		
K ₂ O	1.73	1.66	1.79	0.90	1.50	1.32	3.39	1.60	3.72	3.85		
F	0.16	BDL	BDL	0.12	0.15	0.28	BDL	BDL	0.32	BDL		
Cl	BDL	0.08	0.16	0.08	0.09	0.12	BDL	0.10	0.14	0.11		
P ₂ O ₅	0.14	0.54	0.38	0.18	0.18	0.44	0.08	0.34	0.83	0.69		
Total	96.54	98.36	98.09	99.38	99.54	96.32	97.04	100.2	96.47	98.94		
Ca/K	3.00	3.79	3.20	9.86	5.00	3.97	0.49	4.93	0.96	0.70		
Cl/K	<0.008	0.064	0.119	0.118	0.080	0.121	<0.039	0.083	0.050	0.038		

Notes: BDL = below detection limit. All data are given in weight percent.

Table T2. ⁴⁰Ar-³⁹Ar data on milligram-sized fractions.

Laser power (W)	³⁶ Ar _(atm)	³⁷ Ar _(Ca)	³⁸ Ar _(Cl)	³⁹ Ar _(K)	⁴⁰ Ar _(Total)	Age (Ma)	± 2 σ	⁴⁰ Ar*%	³⁹ Ar _(K) %	Ca/K	Cl/K
178-1097A-27R-1, 35–58 cm, (6.8 mg) <i>J</i> = 0.0006101											
0.08	0.5065	0.07628	0.00022	0.5295	203.02	107.6	7.1	26.3	4.8	0.272	0.00029
0.13	0.6018	0.1418	—	0.6239	287.90	184.4	4.3	38.2	5.6	0.429	—
0.15	0.2365	0.1259	0.00754	0.5314	171.28	198.7	6.9	59.2	4.8	0.447	0.00972
0.20	0.1187	0.1715	0.00149	0.6055	129.58	164.1	4.7	72.9	5.4	0.534	0.00169
0.25	0.09528	0.2114	—	0.6324	107.03	132.3	1.6	73.7	5.7	0.631	—
0.30	0.08558	0.2501	0.00117	0.6553	102.31	124.9	1.4	75.3	5.9	0.720	0.00123
0.35	0.06339	0.2577	0.00041	0.5202	76.382	118.0	1.0	75.5	4.7	0.935	0.00054
0.45	0.06109	0.3246	0.00058	0.4733	69.118	115.00	0.83	73.9	4.3	1.29	0.00084
0.60	0.06048	0.4942	0.00131	0.5502	75.897	112.47	0.78	76.4	4.9	1.69	0.00163
0.75	0.02948	0.5939	0.00148	0.5500	67.078	113.17	0.67	87.0	4.9	2.04	0.00184
0.90	0.01465	0.4952	0.00187	0.4605	53.084	112.9	1.0	91.8	4.1	2.03	0.00278
1.10	0.01006	0.4256	0.00157	0.3930	44.343	112.3	1.1	93.3	3.5	2.04	0.00273
1.40	0.01494	0.6543	0.00375	0.6838	71.918	105.49	0.72	93.9	6.1	1.81	0.00376
1.70	0.00994	0.4497	0.00217	0.4855	48.773	101.02	0.85	94.0	4.4	1.75	0.00307
2.60	0.00815	0.5518	0.00367	0.5497	53.683	99.85	0.88	95.5	4.9	1.89	0.00458
3.60	0.01705	1.0199	0.00540	0.9635	96.192	101.22	0.62	94.8	8.7	2.00	0.00384
5.50	0.01836	1.3583	0.00537	0.9619	95.001	99.67	0.53	94.3	8.6	2.66	0.00382
Fuse	0.04297	3.7023	0.01073	0.9528	111.74	110.9	3.4	88.6	8.6	7.33	0.00772
Total fusion						121.92	0.95			1.92	0.00300
178-1103A-36R-3, 4–8 cm (10.7 mg) <i>J</i> = 0.0006055											
0.08	0.7636	0.3982	0.07294	0.5833	261.36	65.7	6.2	13.7	2.5	1.29	0.0856
0.13	0.1923	0.3108	0.04580	0.4830	63.961	16.0	1.4	11.1	2.1	1.21	0.0650
0.18	0.2051	0.6588	0.07713	0.9566	74.588	15.89	0.34	18.7	4.1	1.30	0.0552
0.22	0.07506	0.4938	0.05619	0.7571	35.201	18.69	0.43	37.0	3.2	1.23	0.0508
0.30	0.1462	1.0358	0.09445	1.3786	67.210	18.92	0.33	35.7	5.9	1.42	0.0469
0.35	0.06298	0.9182	0.07011	1.0602	38.180	20.05	0.52	51.2	4.5	1.63	0.0453
0.45	0.06697	1.2394	0.09074	1.2766	43.523	20.20	0.46	54.5	5.4	1.83	0.0487
0.55	0.06117	1.2327	0.07837	1.1887	39.649	19.72	0.50	54.4	5.1	1.96	0.0452
0.70	0.05123	1.3936	0.07764	1.1721	35.807	19.16	0.42	57.7	5.0	2.24	0.0454
0.90	0.07611	2.3047	0.1084	1.7368	54.257	19.87	0.27	58.5	7.4	2.50	0.0428
1.10	0.03768	1.4264	0.06051	0.9939	28.573	19.06	0.50	61.0	4.2	2.71	0.0417
1.60	0.1014	3.3451	0.1128	1.9914	70.534	22.12	0.30	57.5	8.5	3.17	0.0388
1.90	0.02449	0.8622	0.03147	0.5473	17.954	21.3	1.5	59.7	2.3	2.97	0.0394
2.60	0.02572	0.7042	0.02622	0.4567	16.310	20.7	1.7	53.4	1.9	2.91	0.0393
3.20	0.1533	3.1166	0.09724	1.5713	73.572	19.54	0.54	38.4	6.7	3.74	0.0424
3.70	0.08756	1.9973	0.05948	0.9816	43.246	19.23	0.86	40.2	4.2	3.84	0.0415
4.20	0.04822	1.2277	0.03612	0.5909	25.074	19.90	0.70	43.2	2.5	3.92	0.0419
6.50	0.1762	5.8179	0.1266	1.9562	88.240	20.09	0.34	41.0	8.3	5.61	0.0443
Fuse	0.3797	12.044	0.1998	3.7537	203.49	26.37	0.47	44.9	16.0	6.05	0.0365
Total fusion						21.89	0.24			3.26	0.0445

Notes: Argon data x 10⁻¹⁵ moles. — = undetectable.

Table T3. ⁴⁰Ar-³⁹Ar data on multi-grain fractions. (See table notes. Continued on next page.)

Laser power (W)	³⁶ Ar _(atm)	³⁷ Ar _(Ca)	³⁸ Ar _(Cl)	³⁹ Ar _(K)	⁴⁰ Ar _(Total)	Age (Ma)	±2 σ	⁴⁰ Ar*%	³⁹ Ar _(K) %	Ca/K	Cl/K
178-1097A-27R-1, 35–58 (10 grains) <i>J</i> = 0.0006101											
0.30	0.01374	0.01450	0.000439	0.03466	8.5112	136.0	2.5	52.3	43.0	0.789	0.00867
2.50	0.00133	0.03723	0.000143	0.02990	3.3837	106.9	3.3	88.4	37.1	2.350	0.00328
Fuse	0.00051	0.04146	0.000163	0.01609	1.6506	99.7	5.7	90.8	19.9	4.86	0.00692
Total fusion (1)						118.1	2.2			2.18	0.00632
0.30	0.01404	0.00830	0.000314	0.03309	8.4940	139.0	5.5	51.2	56.9	0.473	0.00650
2.50	0.00119	0.03091	0.000052	0.01802	2.0829	102.8	3.2	83.1	31.0	3.24	0.00196
Fuse	0.00042	0.03406	0.000071	0.00709	0.6157	74.9	8.7	80.0	12.2	9.06	0.00688
Total fusion (2)						120.1	3.5			2.38	0.00051
0.30	0.02017	0.01207	—	0.03612	11.519	161.9	5.7	48.2	29.6	0.631	—
2.50	0.00180	0.05099	0.000067	0.07003	7.2389	102.4	1.1	92.6	57.4	1.37	0.00066
Fuse	0.00046	0.05466	0.000038	0.01578	1.5827	98.2	4.2	91.4	12.9	6.54	0.00165
Total fusion (3)						119.7	2.0			1.82	0.00059
0.30	0.02409	0.02868	0.000092	0.02794	11.149	152.1	4.8	36.1	45.2	1.94	0.00225
2.50	0.00183	0.02217	0.000069	0.02346	3.0580	114.4	3.5	82.3	38.0	1.78	0.00202
Fuse	0.00054	0.05684	0.000241	0.01038	1.0980	97.0	4.8	85.6	16.8	10.3	0.01591
Total fusion (4)						128.7	2.7			3.29	0.00446
0.30	0.02450	0.01838	0.000358	0.05449	13.852	128.9	5.0	47.7	35.1	0.636	0.00449
2.50	0.00307	0.07396	0.000060	0.07290	10.531	139.7	1.9	91.4	47.0	1.91	0.00057
Fuse	0.00172	0.06871	0.000382	0.02773	5.0944	173.4	4.5	90.0	17.9	4.68	0.00944
Total fusion (5)						142.0	2.3			1.96	0.00353
178-1103A-36R-3, 4–8 (30 grains) <i>J</i> = 0.0006055											
0.30	0.02190	0.17832	0.01513	0.1689	9.0580	16.65	0.77	28.6	41.5	1.99	0.0614
2.50	0.01486	0.36118	0.01043	0.1671	6.4099	13.2	1.1	31.5	41.0	4.08	0.0427
Fuse	0.00630	0.27847	0.00486	0.07110	3.3325	22.5	1.2	44.1	17.5	7.39	0.0468
Total fusion (1)						16.23	0.59			3.79	0.0512
0.30	0.02043	0.15718	0.01710	0.2049	8.8648	15.02	0.91	31.9	42.1	1.45	0.0572
2.50	0.00616	0.32642	0.01194	0.2089	6.1354	22.43	0.47	70.3	42.9	2.95	0.0391
Fuse	0.00306	0.18759	0.00398	0.07323	2.4822	23.4	1.1	63.5	15.0	4.83	0.0373
Total fusion (2)						19.46	0.48			2.60	0.0465
0.30	0.04537	0.12835	0.01421	0.1702	15.534	13.6	2.9	13.7	38.5	1.42	0.0572
2.50	0.00773	0.18650	0.02103	0.2715	4.8246	10.19	0.31	52.6	61.5	1.30	0.0531
Total fusion (3)**						11.5	1.1			1.35	0.0547
0.30	0.01987	0.06365	0.00609	0.08790	9.0946	39.6	2.8	35.4	20.8	1.37	0.0475
2.50	0.00767	0.31486	0.01122	0.2565	13.4346	46.95	0.36	83.1	60.8	2.32	0.0300
Fuse	0.00997	0.19887	0.00379	0.07734	5.7798	39.60	0.97	49.0	18.3	4.85	0.0336
Total fusion (4)						44.07	0.71			2.58	0.0343
0.30	0.01496	0.17008	0.01488	0.16764	6.2791	12.07	1.06	29.6	61.6	1.91	0.0608
2.50	0.00514	0.15854	0.00548	0.06959	2.0038	7.58	0.71	24.1	25.6	4.30	0.0540
Fuse	0.00180	0.14358	0.00254	0.03503	0.8175	8.9	1.8	34.8	12.9	7.73	0.0497
Total fusion (5)						10.51	0.72			3.27	0.0576
0.20	0.00184	0.02750	0.00334	0.03966	1.0643	14.3	2.1	48.9	9.1	1.31	0.0578
2.50	0.01212	0.38295	0.01959	0.3174	8.7263	17.62	0.66	58.9	72.4	2.28	0.0423
Fuse	0.00261	0.15455	0.00351	0.08111	2.6734	25.4	1.3	71.1	18.5	3.60	0.0297
Total fusion (6)						18.77	0.58			2.43	0.0413
0.30	0.00381	0.08094	0.00876	0.12325	3.2553	18.77	0.79	65.4	36.9	1.24	0.0487
2.50	0.00789	0.27852	0.00915	0.17038	4.7174	15.23	0.84	50.6	51.0	3.08	0.0368
Fuse	0.00114	0.06187	0.00199	0.04021	0.8526	14.0	1.1	60.5	12.0	2.90	0.0340
Total fusion (7)						16.39	0.54			2.38	0.0408
0.30	0.00784	0.10476	0.00931	0.13349	3.9554	13.4	1.1	41.4	42.3	1.48	0.0478
2.50	0.00434	0.16440	0.00804	0.12308	3.1241	16.3	1.8	59.0	39.0	2.52	0.0447
Fuse	0.00392	0.12439	0.00302	0.05883	1.7934	11.8	2.7	35.4	18.7	3.99	0.0351
Total fusion (8)						14.20	0.97			2.35	0.0442
0.30	0.01589	0.10916	0.00947	0.1407	7.7633	23.7	1.1	39.5	40.6	1.46	0.0461
2.50	0.00805	0.19166	0.00822	0.1372	4.9662	20.48	0.68	52.1	39.6	2.64	0.0410
Fuse	0.00271	0.08859	0.00242	0.06851	3.9967	50.2	1.4	79.9	19.8	2.44	0.0242
Total fusion (9)						27.69	0.59			2.12	0.0398
178-1103A-31R-2, 0–4 cm (30 grains) <i>J</i> = 0.0006015											
0.80	0.05528	0.18844	0.01771	0.2999	21.902	20.03	0.70	25.4	79.2	1.19	0.0404
1.80	0.01147	0.07760	0.00227	0.05063	4.3841	21.2	5.2	22.7	13.4	2.89	0.0307
Fuse	0.00322	0.04598	0.00116	0.02791	2.0102	40.7	2.0	52.7	7.4	3.11	0.0284
Total fusion (1)						21.72	0.91			1.56	0.0383

Table T3 (continued).

Laser power (W)	³⁶ Ar _(atm)	³⁷ Ar _(Ca)	³⁸ Ar _(Cl)	³⁹ Ar _(K)	⁴⁰ Ar _(Total)	Age (Ma)	±2 σ	⁴⁰ Ar*%	³⁹ Ar _(K) %	Ca/K	Cl/K
0.90	0.06668	0.37257	0.02675	0.3651	25.650	17.59	0.68	23.2	67.6	1.93	0.0502
2.40	0.00835	0.12221	0.00520	0.08370	4.2266	22.65	0.80	41.6	15.5	2.76	0.0426
Fuse	0.01026	0.20752	0.00478	0.09120	5.5567	29.8	2.0	45.4	16.9	4.29	0.0359
Total fusion (2)						20.44	0.60			2.45	0.0466
0.40	0.03091	0.11609	0.01054	0.1747	12.691	22.0	1.7	28.0	47.1	1.25	0.0413
2.50	0.01274	0.17526	0.00608	0.1562	6.3921	18.16	0.81	41.1	42.1	2.12	0.0267
Fuse	0.00470	0.06368	0.00210	0.04029	2.2810	23.9	3.1	39.1	10.9	2.98	0.0357
Total fusion (3)						20.58	0.92			1.80	0.0345
0.40	0.05939	0.13952	0.00993	0.1998	24.144	35.47	0.78	27.3	65.9	1.32	0.0340
2.50	0.00478	0.10570	0.00275	0.07833	4.0605	36.3	1.4	65.2	25.8	2.55	0.0240
Fuse	0.00246	0.04932	0.00076	0.02521	1.9288	51.0	5.3	62.3	8.3	3.69	0.0206
Total fusion (4)						36.98	0.80			1.83	0.0303
0.30	0.04550	0.12811	0.01406	0.2473	21.474	34.89	0.86	37.4	41.4	0.98	0.0389
2.50	0.02261	0.26826	0.01300	0.2623	15.501	36.12	0.69	56.9	43.9	1.93	0.0339
Fuse	0.00750	0.11478	0.00321	0.08825	6.9419	57.2	1.4	68.1	14.8	2.45	0.0249
Total fusion (5)						38.74	0.56			1.61	0.0347
0.30	0.02806	0.10043	0.01123	0.1591	11.676	22.9	1.2	29.0	37.3	1.19	0.0483
2.50	0.01684	0.22645	0.00888	0.1960	10.997	33.02	0.47	54.7	46.0	2.18	0.0310
Fuse	0.00551	0.10905	0.00288	0.07129	4.4072	41.8	1.1	63.0	16.7	2.89	0.0277
Total fusion (6)						30.73	0.56			1.93	0.0369
0.30	0.00820	0.05156	0.00727	0.1091	4.5880	21.4	1.1	47.2	28.1	0.891	0.0456
2.50	0.00956	0.21198	0.00940	0.2039	7.5544	24.99	0.76	62.6	52.5	1.96	0.0316
Fuse	0.00388	0.11014	0.00291	0.07534	3.3410	31.3	1.3	65.7	19.4	2.76	0.0265
Total fusion (7)						25.22	0.59			1.82	0.0345
0.30	0.00704	0.07496	0.00578	0.1071	5.2186	31.51	0.80	60.1	39.9	1.32	0.0370
2.50	0.00479	0.17473	0.00591	0.1343	6.2567	38.68	0.89	77.3	50.1	2.45	0.0302
Fuse	0.00148	0.04707	0.00109	0.02677	1.4380	40.1	3.9	69.5	10.0	3.32	0.0280
Total fusion (8)						35.96	0.71			2.09	0.0327
0.30	0.00690	0.08108	0.00761	0.1164	4.2148	20.2	1.3	51.6	45.4	1.31	0.0448
2.50	0.00745	0.14725	0.00604	0.1150	4.4063	20.7	1.3	50.0	44.8	2.42	0.0360
Fuse	0.00181	0.03534	0.00152	0.02524	1.3063	32.9	4.8	59.1	9.8	2.64	0.0414
Total fusion (9)						21.65	0.94			1.94	0.0405
0.30	0.00567	0.09547	0.00780	0.1307	3.8572	18.0	1.2	56.5	45.8	1.38	0.0409
2.50	0.00581	0.15897	0.00508	0.1148	4.3240	24.48	0.91	60.3	40.2	2.61	0.0303
Fuse	0.00200	0.04540	0.00135	0.03992	1.9852	37.5	2.4	70.3	14.0	2.15	0.0231
Total fusion (10)						23.35	0.76			1.98	0.0342
0.30	0.00390	0.04440	0.00399	0.07704	2.9107	24.6	1.9	60.4	33.6	1.09	0.0354
2.50	0.00939	0.16839	0.00617	0.1287	6.3955	30.3	1.3	56.6	56.1	2.47	0.0329
Fuse	0.00119	0.03267	0.00088	0.02378	1.1781	37.4	2.4	70.2	10.4	2.59	0.0252
Total fusion (11)						29.1	1.0			2.02	0.0329

Notes: ** = the final step was lost for a technical reason. Argon data are × 10⁻¹⁵ moles. — = undetectable.